Structure and bonding in TiNiSi type LaMgSnH intermetallic hydride

Yartys, Volodymyr A.; Denys, Roman V.; Akselrud, Lev G.; Vajeeston, Ponniah; Dankelman, Robert; Plomp, Jeroen; Block, Theresa; Pöttgen, Rainer; Wragg, David; More Authors

DOI
10.1016/j.jallcom.2023.173198

Publication date
2024

Document Version
Final published version

Published in
Journal of Alloys and Compounds

Citation (APA)
Yartys, V. A., Denys, R. V., Akselrud, L. G., Vajeeston, P., Dankelman, R., Plomp, J., Block, T., Pöttgen, R., Wragg, D., & More Authors (2024). Structure and bonding in TiNiSi type LaMgSnH intermetallic hydride. *Journal of Alloys and Compounds*, *976*, Article 173198. https://doi.org/10.1016/j.jallcom.2023.173198

Journal of Alloys and Compounds 976 (2024) 173198

Contents lists available at ScienceDirect

Journal of Alloys and Compounds

journal homepage: www.elsevier.com/locate/jalcom

Research Article

Structure and bonding in TiNiSi type LaMgSnH intermetallic hydride

Volodymyr A. Yartys[a,*], Roman V. Denys[a], Lev G. Akselrud[b], Ponniah Vajeeston[c], Robert Dankelman[d], Jeroen Plomp[d], Theresa Block[e], Rainer Pöttgen[e], David Wragg[a], Bruno Guilherme Fischer Eggert[a], Vasyl Berezovets[a,1]

[a] Institute for Energy Technology, P.O. Box 40, Kjeller, NO 2027, Norway
[b] Department of Inorganic Chemistry, Faculty of Chemistry, Ivan Franko National University of Lviv, Kyryla i Mefodiya St., 6, 79005 Lviv, Ukraine
[c] Center for Materials and Nanotechnology, University of Oslo, P.O. Box 1033, NO 0315, Oslo, Norway
[d] Delft University of Technology (TU Delft), Delft Reactor Intituut, Mekelweg 15, Delft 2629, the Netherlands
[e] Institut für Anorganische und Analytische Chemie, Universität Münster, Corrensstrasse 30, 48149 Münster, Germany

ARTICLE INFO

Keywords:
Metal hydrides
LaMgSn stannide
Neutron diffraction
DFT studies
Mössbauer spectroscopy

ABSTRACT

The work was aimed on reaching a better understanding of the effect of magnesium as a component of the hydride-forming LaMgSn intermetallic compound crystallising with the orthorhombic TiNiSi type of structure on the hydrogenation behaviours, crystal structure and bonding interactions with hydrogen. The LaMgSn structure is significantly expanded as compared to the earlier studied isotypic LaNiSn H storage material (volume expansion of 23%), as a result of a substitution of the smaller Ni atoms by much larger Mg atoms. This significantly affects the chemistry of the interaction of the intermetallic compound with hydrogen because a transition metal, Ni, in replaced by an active hydride-forming metal, Mg. The work involved computational studies of the electronic structure of the intermetallic compound and its hydride, and experimental studies of the hydrogenation behaviour and thermal stability of the formed hydride LaMgSnH, its structural characterisation by SR XRD and neutron powder diffraction, and Mössbauer spectroscopic studies of the stannide and its hydride. These studies showed that in the system LaMgSn-H_2 a monohydride LaMgSnH is a thermodynamically favourable hydride composition. PDOS levels show that hydrogen and all constituting elemental metals, La, Mg and Sn, have peaks of electron density in the range between − 6 and − 4 eV indicating their hybridisation. The results show the hybridization of H atoms not only with bonded La and Mg atoms forming H-filled tetrahedra La_3Mg, but also with Sn despite its atoms do not have bonding interactions with H. This explains the high stability of the metal substructure which does not disproportionate into the binary hydrides of La and Mg even when heated to 200 °C @ 20 bar H_2, but instead forms an insertion type hydride. Formation of the monohydride LaMgSnH (Sp.gr. *Pnma*; a=8.1628(4); b= 4.5555(3); c= 9.2391(5) Å; V= 343.56(5) $Å^3$) causes a small (1.26%) expansion of the unit cell volume compared to LaMgSn, and mainly proceeds along the [100] direction. Hydrogen absorption-desorption cycle results in a reversible formation of the initial compound LaMgSn, with the peak of hydrogen release occurring in vacuum at 355 °C, which is intermediate between the temperatures for the vacuum decomposition of the dihydrides MgH_2 and LaH_2. From the combined refinements of the Synchrotron (SR) XRD and Neutron Powder Diffraction (NPD) data, deuterium atoms completely and in an ordered way fill a half of the available La_3Mg interstitial sites with metal-H/D distances of Mg-D= 2.026 Å; La-D= 2.381 and 2.502 Å. The occupied La_3Mg sites are smaller in size than the vacant Mg_3La tetrahedra. Sn and D exhibit a nonbonding interaction with the closest Sn-D separation of 3.033 Å. ^{119}Sn Mössbauer spectra of LaMgSn and LaMgSnH show isomer shifts of 1.98(2) and 1.99(1) mm/s which are typical for the chemically similar stannides.

* Corresponding author.
E-mail address: volodymyr.yartys@ife.no (V.A. Yartys).
[1] Also at Karpenko Physico-Mechanical Institute of the NAS of Ukraine, Lviv, Ukraine.

https://doi.org/10.1016/j.jallcom.2023.173198
Received 30 September 2023; Received in revised form 13 December 2023; Accepted 14 December 2023
Available online 18 December 2023

1. Introduction

Hydrides of equiatomic ternary RTX intermetallics

RTX intermetallic compounds with *R* = Rare Earth Metal; *T* = Transition Metal, Fe, Co, Ni; *X* = Non transition element, Al, Si, Ge, Ga, Sn, In, crystallize with a variety of closely related structure types which can be obtained from the hexagonal AlB_2 type through the ordering of *T* and *X* components and via internal and external deformation of the structures (see Fig. 1a). When the atoms of a transition metal T are substituted by the X atoms in an ordered way, this results in the structures of ZrBeSi, LiGaGe and TiNiSi types (see Fig. 1,b,c,d). These structure types are closely related through group-subgroup relations [1, 2].

The TiNiSi-type structure is one of the most common structure types among the equiatomic *RTX* ternaries. The chemical nature of the constituent elements, rare earth metals R, transitions metals T and non-transition elements X significantly affects their crystal structures, magnetism, hydrogenation and other properties [3–5].

The crystal structure of the *RTX* hydride host structures with an orthorhombic TiNiSi type contain 5 types of interstitial sites shown in the Fig. 2a, which are suitable for the accommodation of hydrogen atoms. The maximum hydrogen storage capacity of the insertion derivative to the TiNiSi type is a dihydride $RTXH_2$. Studies of the crystal structure data for two dihydrides formed on the basis of TiNiSi-type intermetallics, $LaNiSnD_2$ [6] and $TbNiSiD_{1.78}$ [7], showed that independent of *X* (Sn or Si), in both cases a transformation from an orthorhombic TiNiSi to the hexagonal ZrBeSi-type metal matrix (flattening of the [NiSn] substructure) proceeds on deuteration. The D atoms occupy all available R_3Ni (La_3Ni or Tb_3Ni) tetrahedra. Neutron diffraction study of the dihydrides $LaNiSnD_2$ and $TbNiSiD_{1.78}$ showed that the filled by D atoms R_3Ni tetrahedra form a spatial network via connecting to each other by vertexes and edges (see. Fig. 2b).

Further to the TiNiSi→ZrBeSi type rebuilding of the orthorhombic structure into a hexagonal one upon the hydrogenation, the crystal structures of the intermetallic compounds of the orthorhombic TiNiSi type undergo two other types of transformations when accommodating hydrogen atoms, including a) formation of internally deformed orthorhombic CeNiSnD [8], NdNiSnD [9] and TbNiSnD [10] hydride structures; b) TiNiSi→ZrNiAl type reconstructive rebuilding accompanied by a small contraction of the unit cell volume which was observed for the $ScNiSnH_{0.6}$ hydride [11].

During the formation of the monohydrides *R*NiSnD (*R* = Ce, Nd, Tb), the volume expansion is rather small, 1.5%− 2.8%, which is equivalent to a modest specific value of 1.0–1.3 $Å^3$/at.D.

Structural, magnetic and hydrogenation properties of the various Ce- and U-containing ABC intermetallics were described in the reference publications [12–17] which considered a variety of interesting phenomena accompanying the formation of their hydrides.

The present paper focuses on a study of the LaMgSn-based hydride. LaMgSn crystallises with a TiNiSi type structure with the unit cell parameters $a = 7.811$; $b = 4.689$; $c = 9.148$ Å [18].

We wish to study how a change in the chemical composition of the intermetallic alloy (LaNiSn → LaMgSn; Ni → Mg) and in the average size of the interstitial sites available for the accommodation of hydrogen atoms which increases on a replacement of small Ni by large Mg atoms (1.246 → 1.602 Å) affects the hydrogenation behaviours and the properties of the formed hydrides. Indeed, the chemistry of the interaction of the intermetallic compound with hydrogen becomes significantly affected by such a substitution because of a replacement of a transition metal (Ni) by an active hydride-forming metal (Mg). In turn, the volume of the unit cell of the crystal structure of LaMgSn, 335.1 $Å^3$, is significantly larger as compared to LaNiSn, 272.4 $Å^3$ (by 23%), causing a corresponding increase in the size of the interstitial sites for the accommodation of H atoms.

The work involved computational studies of the electronic structure of the intermetallic compound and its hydride, and experimental studies of the hydrogenation behaviour and thermal stability of the formed hydride LaMgSnH, structural characterisation by SR XRD and neutron powder diffraction, and Mössbauer spectroscopic studies of intermetallic compound and its hydride.

2. Experimental

2.1. Initial intermetallic compound

The intermetallic compound LaMgSn was prepared from a mixture of Mg and an arc-melted LaSn precursor sample (purity of the initial metals was higher than 99.9 wt%) which were milled together after being mixed in stoichiometric quantities and pressed into the pellets at 25 MPa. An excess of 4 wt% of Mg was added as compared to the stoichiometric 1:1 mixture of Mg and LaSn to compensate for the sublimation of magnesium during the high temperature synthesis. The pellets were wrapped into a Ta foil and placed into stainless steel tubes. The tubes were sealed by welding in an Ar atmosphere and then annealed at 800 °C for 24 h. After the annealing the samples were quenched into a water-ice mixture. X-ray diffraction (XRD) studies were performed on a Bruker D2 Phaser using monochromated Cu Kα radiation.

2.2. Synthesis of hydride/deuteride

The hydrogenation/deuteration was performed at 200 °C and 20 bar H_2/D_2 after a heat treatment of the intermetallic compound in dynamic vacuum at 350 °C. The hydrogenation reaction lasted about

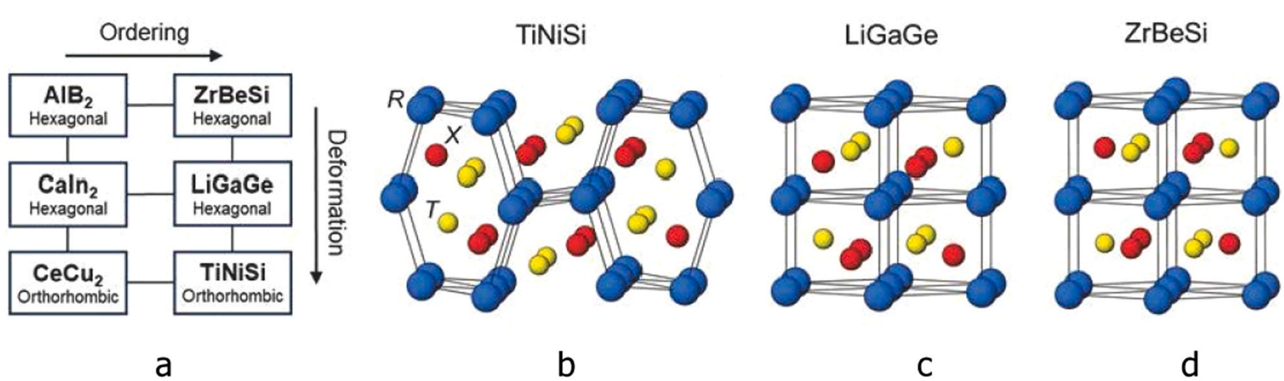

Fig. 1. An overview of the related structure types which for the ABC stoichiometries include the ZrBeSi, LiGaGe and TiNiSi types which are related to the AlB_2, $CaIn_2$ and $CeCu_2$ types of the binary intermetallics (a). Comparison of the different related *RTX* structure types, TiNiSi (b), LiGaGe (c) and ZrBeSi (d). The latter two structures have AA stacking of the close-packed layers of *R* and differ by a displacement of the smaller *T* and *X* atoms, whereas the former is the most distorted structure.

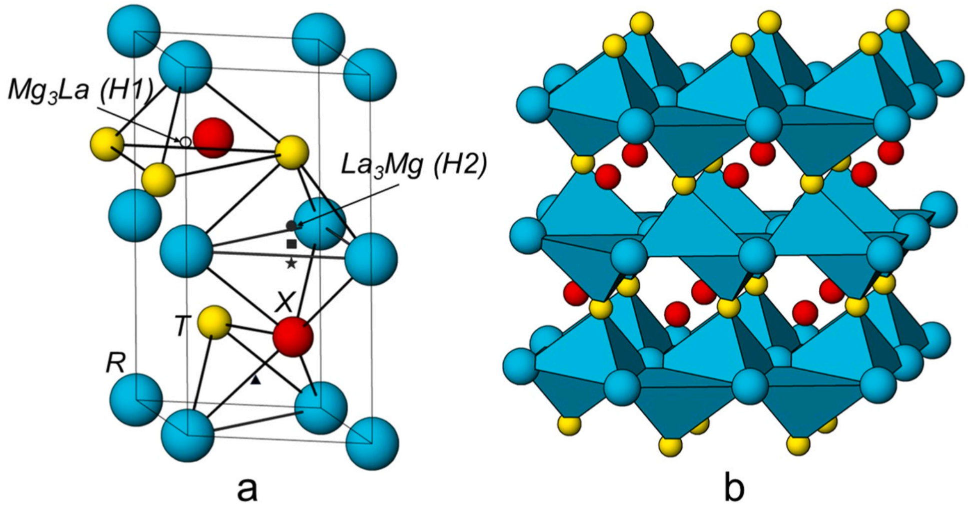

Fig. 2. a) Selected possible hydrogen sites in *RTX* hydride with TiNiSi-type related ZrBeSi-type structure. Interstitial sites: R_3T site (●), R_3TX(■), R_3X (*), R_2TX (▲) and T_3R (◦). The coordination polyhedra are outlined. Mg_3La (H1) and La_3Mg (H2) sites which are discussed in the Chapter 3.1 (Theoretical studies) are highlighted. (b) Structure of $LaNiSnD_2$ [6] illustrated as D (La_3Ni) tetrahedra sharing La–La edges and Ni corners. Isolated Sn atoms do not form bonds with hydrogen.

3 h. To ensure a complete saturation, the sample was kept at at the reaction conditions for 24 h. Hydrogen/deuterium absorption resulted in the synthesis of the $LaMgSn(H/D)_{1.0}$ hydride/ deuteride. The hydrogen content was determined from the changes of gas pressure in a calibrated volume. Approximately 2.615 g of the sample has been used to prepare its deuteride, which has been used during the NPD studies. Deuterium gas used during the synthesis of the deuteride had a purity of 99.9%.

2.3. Thermal desorption spectroscopy

The TDS study was performed at a heating rate of 2 K/min in a temperature interval of 20–550 °C. The sample for the TDS experiment (~300 mg) was loaded inside an Ar glove box into the autoclave made of a ½'' SS316 tubing and equipped with a port for K-type thermocouple. The pressure for starting the measurements was 1×10^{-5} mbar and was provided by a turbomolecular pump. During the gas evolution in the course of the TDS studies, the gas pressure at the entrance of the turbomolecular pump, was measured by Pirani-Penning vacuum sensor and was between $3 * 10^{-5}$ and $2 * 10^{-2}$ mbar; thus, the pressure drop related to the flow of the evacuated H_2 can be considered to be equal to the display of the vacuum sensor. Further calibration allowed to calculate the H_2 desorption flow ($Ncm^3min^{-1}g^{-1}$) from the measurements data of the Pirani-Penning sensor during the TDS experiments. The TDS measurements were performed in a sequence described in our earlier publication (see Table 1 in [19]). Use of the TDS spectrum allowed to accurately determine the amount of hydrogen released during the desorption experiments.

2.4. Powder diffraction studies

XRD examination of the intermetallic compound was performed using a Bruker D2 Phaser diffractometer with Cu K-α (λ = 1.5406 Å) radiation in Bragg-Brentano configuration and showed the formation of a high purity TiNiSi-type LaMgSn intermetallic compound. SR XRD was collected at beamline BM01, SNBL, ESRF, Grenoble, France, using a wavelength of 0.75334 Å (LaMgSn) and 0.71073 Å (LaMgSnH). The powdered samples were sealed in 0.3 mm glass capillaries. The instrument used to collect the data and the azimuthal integration method used on the 2D detector images are described in [20]. The refinements of the SR XRD data (Fig. S1; Table S1) yielded the unit cell parameters of a = 7.8482(1); b = 4.70977(7); c = 9.1795(1) Å; V = 339.30(2) $Å^3$ which are slightly larger as compared to the reference data (see the Supplementary Information file for further details on the crystal structure data).

NPD data was collected at the 2 MW research reactor of Delft University of Technology (Netherlands) using a PEARL diffractometer [21] and a wavelength of 1.67 Å obtained with a Ge monochromator. The powdered sample, around 2 g, was hermetically sealed in a vanadium 6 mm ILL type sample holder.

The refinements of the SR XRD and NPD pattern were performed using WinCSD software package [22].

Table 1
Crystallographic data for LaMgSn, its monohydride LaMgSnH and the sample $LaMgSnH_{\sim 0}$ after hydrogen release.

	LaMgSn	LaMgSnH	Change, %	$LaMgSnH_{\sim 0}$
a, Å	7.8482(1)	8.1628(4)	4.01	7.8155(4)
b, Å	4.70977(7)	4.5555(3)	-3.28	4.6825(2)
c, Å	9.1795(1)	9.2391(5)	0.65	9.1297(5)
V, $Å^3$	339.30(2)	343.56(5)	1.26	334.11(3)

2.5. ^{119}Sn Mössbauer spectroscopy

A $Ca^{119m}SnO_3$ source was used for the ^{119}Sn Mössbauer spectroscopic experiments on LaMgSn and its hydride LaMgSnH. Source, sample and detector were arranged in the usual transmission geometry. To reduce the tin K X-rays emitted by this source a palladium foil (0.05 mm) was inserted in front of the detector. Due to the high moisture sensitivity, the preparation of the sample was performed in a glove box to avoid any contamination. The samples were mixed with α-quartz and placed inside thin-walled PMMA containers at a thickness corresponding to about 10 mg Sn per cm^2. They were subsequently cooled to 78 K using a commercial liquid nitrogen-bath cryostat, while the source was kept at room temperature. The counting time for each spectrum was about three days. Fitting and plotting of the spectra were performed with the WinNormos for Igor6 program package [23] and graphical editing with the program CorelDRAW2017 [24].

2.6. Theoretical studies of the electronic structures

Total energies were computed using the projected augmented plane wave (APW) implementation within the Vienna ab initio simulation package (VASP) [25–28]. The Perdew, Burke, and Ernzerhof (PBE) exchange-correlation functional was employed for these calculations [29]. The interaction involving core and valence electrons was described using the projector augmented wave (PAW) method [30,31]. Ground-state geometries were determined through stress and Hellman-Feynman force minimization, utilizing the conjugate gradient algorithm with a force convergence threshold of less than 10^{-3} eV Å^{-1}. During all relaxation processes, Brillouin zone integration was carried out employing a Gaussian broadening of 0.1 eV. Our analysis indicated that 1280 k-points uniformly distributed across the entire Brillouin zone, using a 600 eV plane wave cutoff, ensured optimal accuracy for the calculated results. These k-points were generated using the Monkhorst-Pack method with a 10 × 16 × 8 grid for structural optimization. A commensurate k-point density and energy cutoff were applied to determine the total energy as a function of volume for all considered structures. The iterative relaxation of atomic positions was terminated when the change in total energy between consecutive steps was less than 1 meV per cell.

3. Results and discussion

3.1. Theoretical studies of the electronic structure of LaMgSn and its hydride LaMgSnH

The total and site-projected electronic density of states (DOS) at the equilibrium volumes for LaMgSn, and for the hypothetical mono- and dihydrides LaMgSnH and $LaMgSnH_2$ phases are presented in Fig. 3, a-c. Furthermore, the orbital-projected DOS for the all the studied phases are shown in Fig. 4. Each of the studied phases exhibits a finite number of electrons at the Fermi energy (E_F). The number of electrons at the E_F varies from 2.67 states/eV for LaMgSn to 0.21 states/eV in LaMgSnH and 1.53 states/eV in $LaMgSnH_2$.

Among the three studied phases, the monohydride LaMgSnH displays a lower metallicity than the other two phases, LaMgSn and $LaMgSnH_2$. A characteristic feature of the total DOS in the LaMgSnH

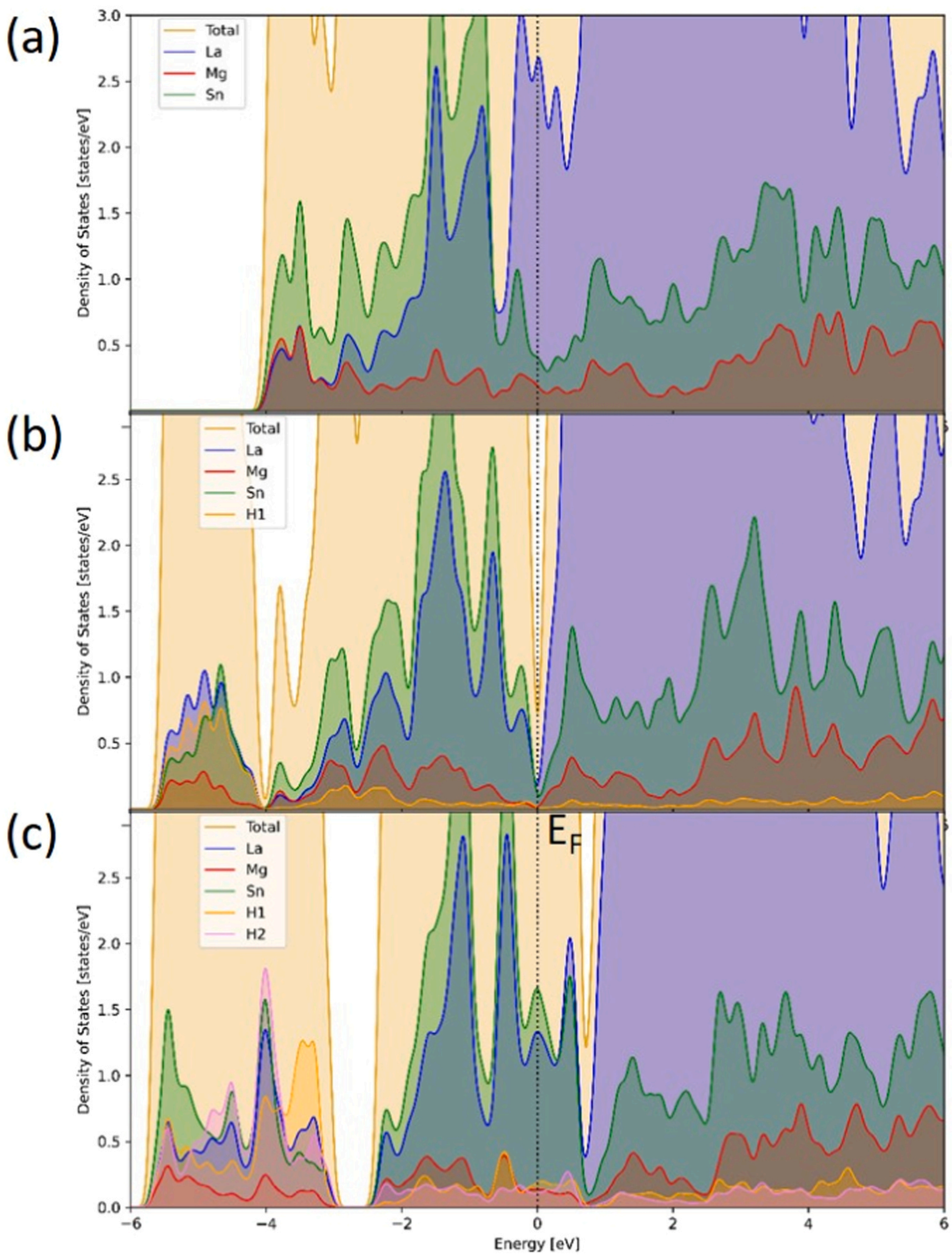

Fig. 3. Calculated total and site projected density of states for LaMgSn (a), LaMgSnH with H filling the La_3Mg tetrahedra (b), and $LaMgSnH_2$ with H equally filling La_3Mg and $LaMg_3$ tetrahedra (c). The Fermi level (E_F) is set to zero energy.

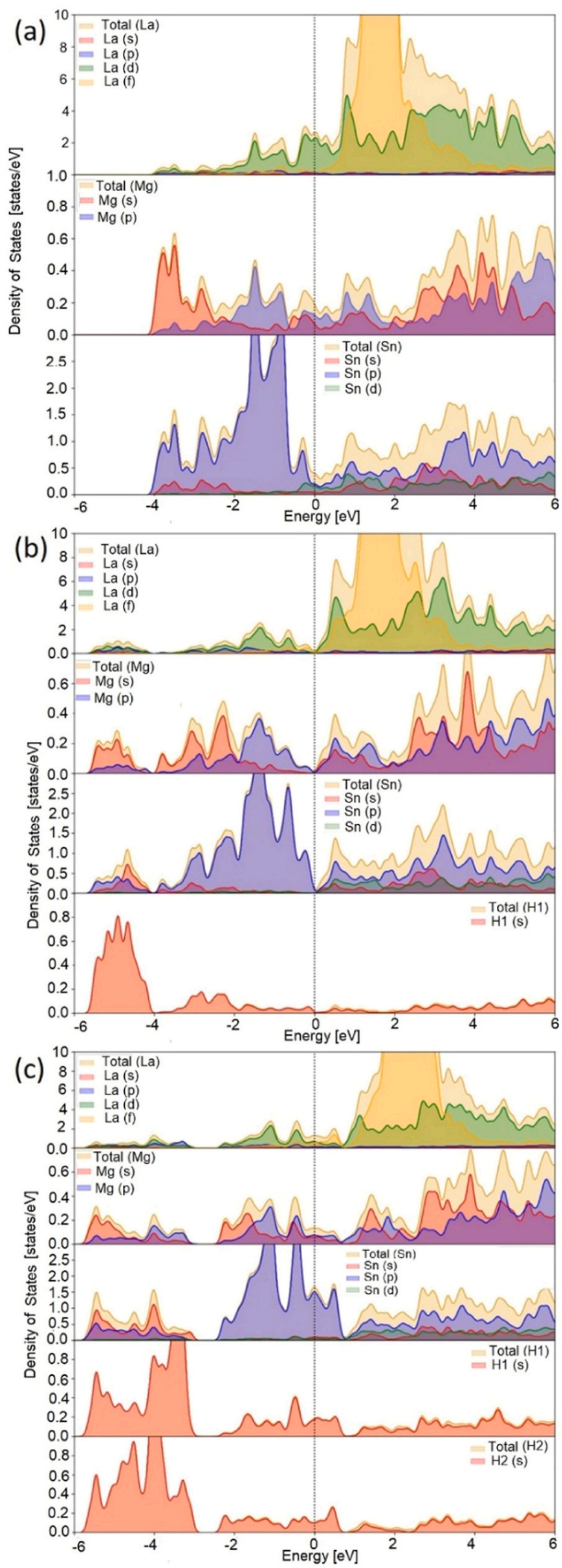

Fig. 4. Calculated orbital projected density of states for LaMgSn (a), LaMgSnH (b), and $LaMgSnH_2$ (c). The Fermi level (E_F) is set to zero energy.

hydride is the presence of what is referred to as a pseudogap, characterized by a sharp valley around the Fermi energy [32]. Two mechanisms have been proposed to explain the formation of this pseudogap in binary alloys: one is of ionic origin, and the other one is attributed to hybridization effects. In LaMgSnH, the H, La, Mg and Sn hybrid states peaking between − 6 and − 4 eV exhibit a significant localization which is more pronounced as compared to LaMgSn and $LaMgSnH_2$.

3.2. Formation energy

We calculated the formation energy of the studied phases (Fig. 5) in order to compare the relative stability of the studied compounds. This has been done using the following expression written for the LaMgSn intermetallic, which has been chosen as an example:

$$\Delta H = E(LaMgSn) - [E(La) + E(Mg) + E(Sn)] \quad (1)$$

Here, E(LaMgSn), E(La), E(Mg), and E(Sn) represent the total energies of the bulk LaMgSn, La, Mg, and Sn, respectively. The results are depicted in Fig. 5. From the calculations, it is evident that LaMgSnH is the most thermodynamically stable compound as compared to LaMgSn or $LaMgSnH_2$ phases. To determine the stable position of hydrogen (H) within LaMgSnH, we explored three different structural models:

- H atom placed in a tetrahedral Mg_3La H1 site (0.56, 1/4, 0.58; $r = 0.72$ Å) (referred to as LaMgSnH (a)). This Mg_3La (H1) site is highlighted in Fig. 2 where it is labelled as T_3R site (◦);
- H in a tetrahedral site La_3Mg H2 site ((0.05; 1/4; 0.40; $r = 0.54$ Å) (referred to as LaMgSnH (b)). This La_3Mg (H2) site is highlighted in Fig. 2 where it is labelled as R_3T site (•);
- Partially occupied H1 and H2 sites (H in sites H1 and H2 with a 50% occupancy, labelled as LaMgSnH (mix)).

Among these models, we found that the hydride with H in the H2 site is highly stable as compared to the other options. This observation is consistent with the results obtained from the NPD study. It is interesting that the size of the preferred H2 La_3Mg site, $r = 0.54$ Å, is smaller as compared to a rather "loose" H1 Mg_3La site, $r = 0.72$ Å.

As the heat of formation of LaMgSnH from LaMgSn is negative, we conclude that LaMgSnH is more thermodynamically stable than LaMgSn.

Two complementary features cause the observed behaviours. These include.

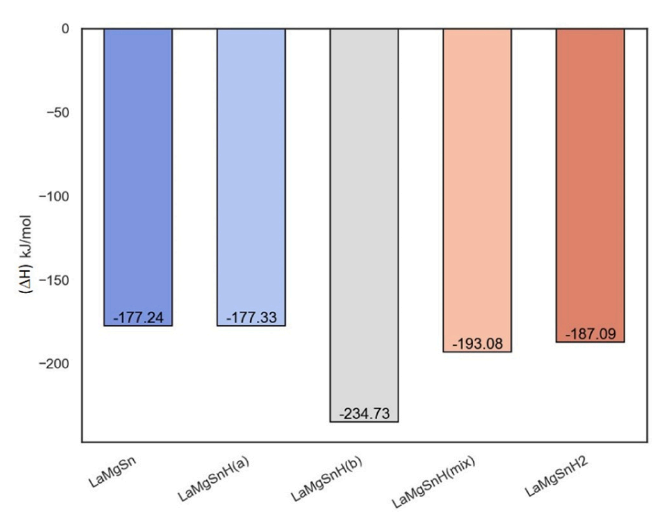

Fig. 5. Calculated formation energy (ΔH) for LaMgSn, LaMgSnH [LaMgSnH (a) - H in a tetrahedral Mg_3La site, LaMgSnH (b)- H in a tetrahedral La_3Mg site, and LaMgSnH(mix)- H in both tetrahedral sites with an equal occupancy], and a hypothetical $LaMgSnH_2$.

(a) Formation of stronger chemical bonds. Indeed, in LaMgSnH the chemical bonds between the constituting elements become stronger as compared to LaMgSn. This is because further to the bonds between the metallic elements, very strong Me-H bonds (La-H and Mg-H) are formed in addition. More energy is released during the formation of these strong bonds resulting in a more negative heat of formation of LaMgSnH as compared to LaMgSn.

(b) Thermodynamic favourability of the hydride formation. Thermodynamics of the multicomponent systems determines the stability of the formed compounds. As the interaction of hydrogen with LaMgSn yielding LaMgSnH is thermodynamically favourable as compared to the system La+Mg+Sn and H_2 with no hydride formed, this will result in a negative heat of formation and a greater stability of LaMgSnH. As the formation of intermetallic hydrides proceeds because of their negative heats of formation, thus, in general hydrides are more stable compounds as compared to the intermetallic alloys.

3.3. Synthesis and thermal desorption spectroscopy study of LaMgSnH

The LaMgSn-hydrogen interaction resulted in the synthesis of the monohydride LaMgSnH. The hydride was thermally stable and decomposed in vacuum showing a broad and symmetrical peak of hydrogen evolution with a maximum at 355 °C (Fig. 6). The peak temperature is higher as compared to the magnesium hydride, showing a peak of hydrogen desorption at 310 °C [33], but much lower as compared to lanthanum dihydride, peaking at 800 °C [34] (see Fig. 6). Furthermore, hydrogen evolution from LaMgSnH proceeds at higher temperatures as compared to LaNiSnH2, 250–340 °C [6] (see Fig. 6 for the details).

These observations indicate that both lanthanum and magnesium atoms should be involved into the formation of the interstitial sites accommodating H atoms in the structure of LaMgSnH. This conclusion accounts the facts that a) The structure of LaMgSn contains two types of tetrahedra jointly formed by La and Mg, La_3Mg and $LaMg_3$ (see Fig. 2), while in the studied structure the interstices solely formed by La or Mg are not available; b) In the intermetallic hydrides, Sn never exhibits bonding interactions with hydrogen, as Sn-containing interstices are not occupied by H atoms in any of the known ternary hydrides.

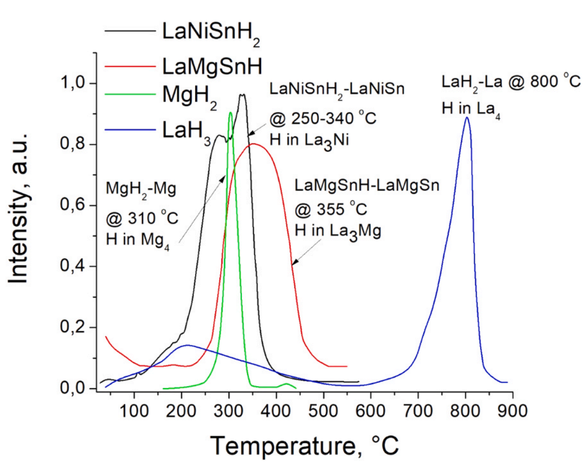

Fig. 6. Thermal Desorption Spectroscopy spectrum of LaMgSnH measured at a heating rate of 2 K/min showing a peak of hydrogen desorption at 355 °C, with an onset of the desorption at 220 °C and its completion at 500 °C. The TDS data for MgH_2 [33], LaH_3 [34] and $LaNiSnH_2$ (peak of hydrogen desorption at 250–340 °C) [6] are presented as a reference and show that a decomposition of LaMgSnH proceeds at higher temperatures as compared to MgH_2 and $LaNiSnH_2$ while at a significantly lower temperature as compared to LaH_2. We note that the decomposition of LaH_3 is a two-step process, with a transformation $LaH_3 \rightarrow LaH_2$ spanning a broad temperature range between 100–500 °C while dihydride LaH_2 decomposes to La metal at high temperatures and this process peaks at 800 °C.

3.4. Crystal structure of LaMgSnD from SR XRD and NPD studies

Rietveld refinements of the SR XRD pattern shown in Fig. 7 resulted in an excellent fit (R_p = 0.0848) and showed a formation of a single phase TiNiSi-type hydride with the parameters of an orthorhombic unit cell (Sp.gr. *Pnma*) of *a*= 8.1628(4); *b*= 4.5555(3); *c*= 9.2391(5) Å.

The hydrogenation / deuteration does not change the TiNiSi type metal substructure. Hydrogen absorption is accompanied by a slight volume expansion, 1.26% (see Table 1). The expansion mostly proceeds along the [100] direction, appr. 4%. At the same time, expansion is very small along [001], while a contraction of the unit cell takes place along [010].

After the TDS was accomplished at 560 °C, the hydride releases all absorbed hydrogen, as this follows from the refinements of the XRD pattern (Fig. 8) and TDS study (Fig. 6).

Neutron powder diffraction pattern were collected for the monodeuteride LaMgSnD. Their indexing showed that the unit cell and the TiNiSi type of the crystal structure remain unaltered indicating that the deuterium sublattice has the same symmetry as the metal atoms. The joint refinements of the SR XRD and NPD pattern showed an excellent fit (see Fig. 9; R_p=0.0856) and concluded that D atoms are completely filling one type of positions – the La_3Mg tetrahedra.

The crystal structure data of LaMgSnD are given in the Table 2.

The crystal structure of LaMgSnD is shown in Fig. 10. The D-occupied La_3Mg tetrahedra are connected by vertexes and by edges. One half of the tetrahedra occupied by D atoms in the structure of $LaNiSnD_2$ is filled in an ordered way.

In the D@La_3Mg tetrahedra, the bonding distances metal-H are Mg–D, 2.026(7); La–D, 2.381(3); La–D, 2 × 2.502(2) Å. Sn and D show a non-bonding interaction with the shortest Sn–D distance of 3.033(4) Å. For comparison, the shortest interatomic distances in the structure of $LaNiSnD_2$ [3] are: La–D, 2.6118(5) Å; Ni–D, 1.619(2) Å and Sn–D, 2.718 (2) Å. In both hydrides the shortest D–D separations are well above 2 Å (2.943(5) Å in the studied structure of LaMgSnD and 2.780(2) Å in the structure of $LaNiSnD_2$ [6]).

Recently, a chemically related but structurally different [35] hydride has been studied by Prof. Vitalij K. Pecharsky and coworkers [35]. Similar to the present work, a close composition-structure-property interrelation has been revealed. Further work on the studies of the behaviour of multicomponent intermetallics as hydrogen storage materials will help to refine the guiding principles allowing to identify metal hydrides with the desired application properties and to optimise their performance.

3.5. Mössbauer spectroscopic characterization

The ^{119}Sn Mössbauer spectra (78 K data) of the stannide LaMgSn and its hydride LaMgSnH are presented in Fig. 11 along with transmission integral fits. The corresponding fitting parameters are summarized in Table 3. In agreement with the data derived from the diffraction experiments, also the ^{119}Sn Mössbauer spectra revealed single tin sites for both samples. As a consequence of the non-cubic site symmetry, both spectra are subjected to electric quadrupole splitting. The line width parameters are in the usual range observed for stannides [36].

The isomer shift is a measure for the *s* electron density at the tin nuclei. An increasing isomer shift corresponds to an increasing *s* electron density as is the case in going from $CaRhSn_2$ to $CaPdSn_2$ [37] and other pairs of stannides. For the currently studied pair LaMgSn / LaMgSnH we observe no change in the isomer shift within one combined standard deviation, indicating almost similar electron density at the tin nuclei.

In a Zintl conform manner one can write an electron-precise formula $La^{3+}Mg^{2+}Sn^{4-}\cdot e^-$ for the ternary stannide accommodating the excess electron in the conduction band vs. $La^{3+}Mg^{2+}Sn^{4-}H^-$ for the hydride. This is in excellent agreement with the densities of states (*vide ultra*), revealing residual DOS for the stannide (i.e. a metallic conductor) and pseudo-gap formation for LaMgSnH; thus the enhanced stability of the

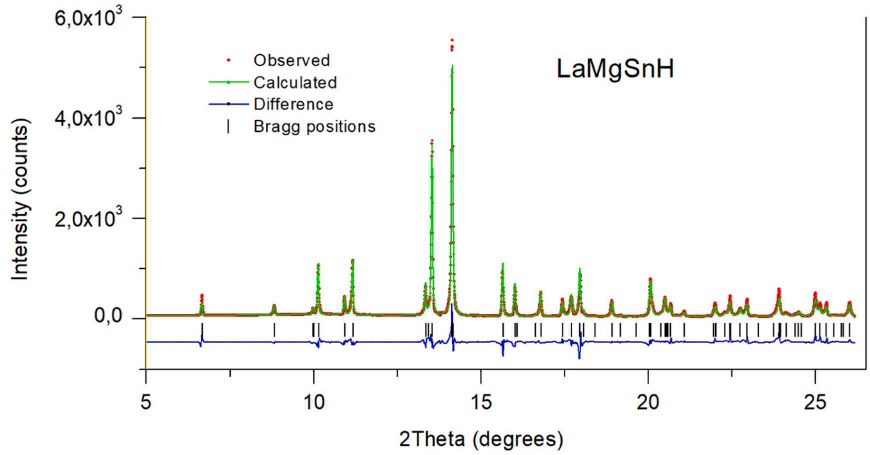

Fig. 7. SR XRD pattern of LaMgSnH measured with a multipurpose diffractometer PILATUS at BM01, SNBL, ESRF, Grenoble, France BM01 with a wavelength of 0.71073 Å. $R_p = 0.0848$.

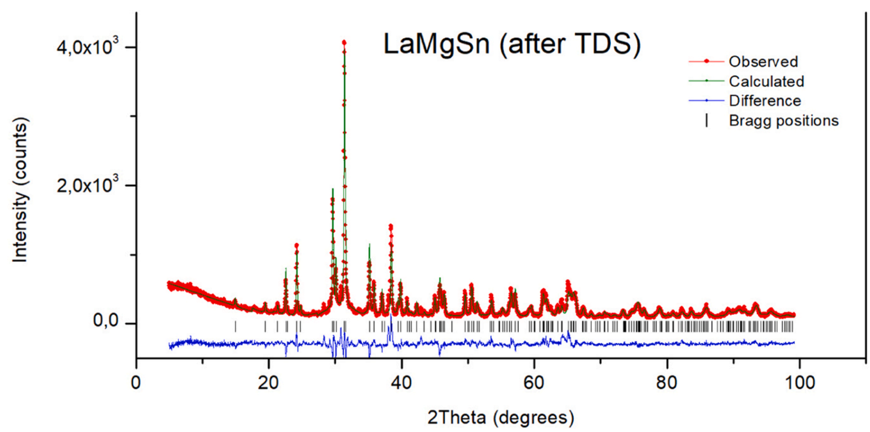

Fig. 8. Rietveld refinement of the XRD pattern of LaMgSn after a complete hydrogen desorption from the hydride LaMgSnH: $a = 7.8155(4)$; $b = 4.6825(2)$; $c = 9.1297(5)$ Å; $V = 334.11(3)$ Å^3; $R_p = 0.0894$. The unit cell parameters are slightly lower as compared to the initial LaMgSn intermetallic sample indicating a loss of Mg because of a very high temperature used to complete the hydrogen desorption, 560 °C, causing a formation of a slightly understoichiometric $LaMg_{1-x}Sn$.

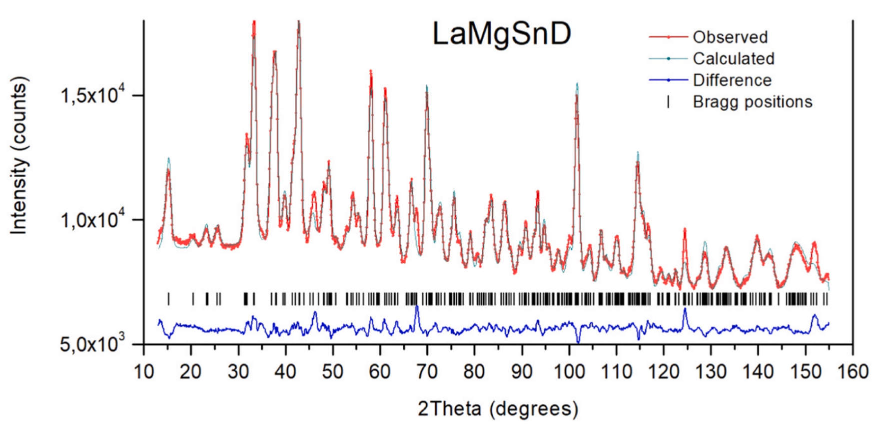

Fig. 9. Rietveld refinement of the NPD pattern of LaMgSnD collected using a PEARL diffractometer at a wavelength of 1.67 Å at the TU Delft Reactor. R_p= 0.0856.

monohydride. The tin is thus not involved in the hydrogenation process. The excess electron is simply transferred from the conduction band to the hydrogen atom and trapped there in the form of $H^{\delta-}$.

Finally, it is interesting to compare the isomer shifts of the pair LaMgSn/LaMgSnH with those of related equiatomic stannides (Table 4). Among the stannides listed in the Table, LaMgSn and its hydride definitely have the highest ionic bonding contribution and consequently we observe the highest electron density at the tin nuclei, i.e., the highest isomer shifts. For the transition metal containing stannides, the isomer shift depends on the varying electron count (substitution of the transition metal). The rhodium and iridium phases (with one valence electron less than the nickel and palladium compounds) show slightly reduced isomer shifts.

Ingoing to the hydrides we observe three different binding situations:

Table 2
Atomic parameters for the deuteride LaMgSnD, space group *Pnma* (No. 62), $a = 8.1628(4)$; $b = 4.5555(3)$; $c = 9.2391(5)$ Å. $V = 343.56(5)$ Å^3. $R_p = 0.0856$.

Atom	Position	x/a	y/b	z/c	B (is/eq), Å^2
La	4*c*	-0.0154(2)	1/4	0.6707(2)	0.93(2)
Mg	4*c*	0.3266(5)	1/4	0.4305(2)	2.07(5)
Sn	4*c*	0.2049(2)	1/4	0.1180(3)	1.11(4)
D	4*c*	0.0784(7)	1/4	0.4267(3)	3.72(6)

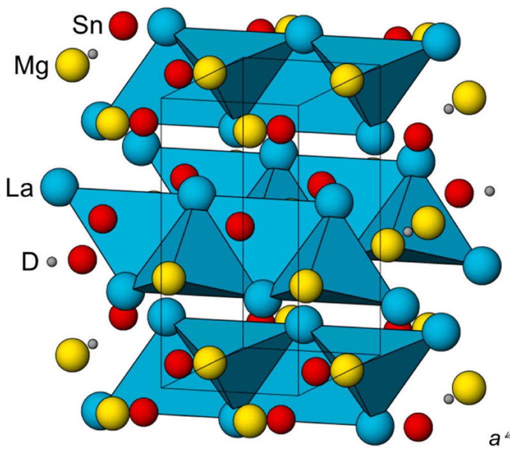

Fig. 10. The crystal structure of LaMgSnD. Occupied by D atoms La_3Mg tetrahedra are connected by vertexes and edges forming the columns aligned along [010].

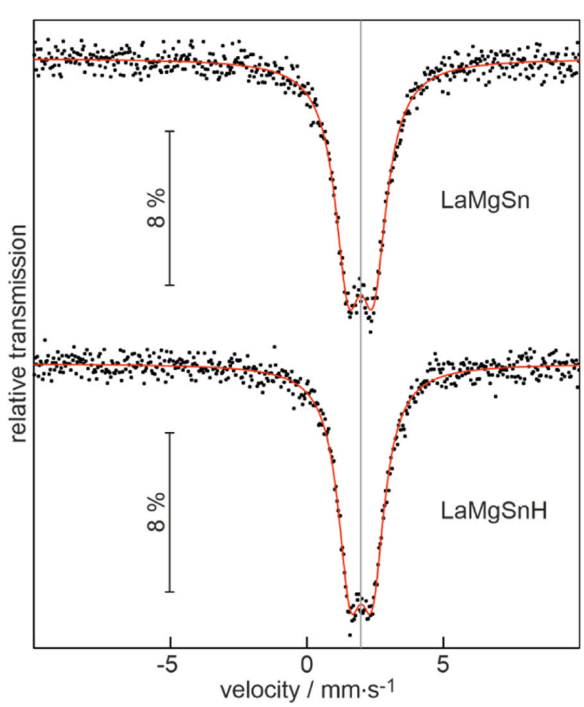

Fig. 11. Experimental (dots) and simulated (blue lines) ^{119}Sn Mössbauer spectra of LaMgSn (top) and LaMgSnH (bottom) measured at 78 K. They red line serves as a guide to the eye.

(i) a decrease of the isomer shift ($ScNiSnH_{0.5}$); (ii) a constant isomer shift (LaMgSnH); and (iii) an increasing isomer shift ($LaNiSnH_2$, CeNiSnH, $CeRhSnH_{0.8}$, CePdSnH, $CeIrSnH_{0.7}$). Thus, the *s* electron density is reduced in $ScNiSnH_{0.5}$, remains constant in LaMgSnH and increases in the remaining hydrides; however, the few examples with different

Table 3
Fitting parameters of ^{119} Sn Mössbauer spectroscopic measurements of LaMgSn and LaMgSnH at 78 K. δ = isomer shift, ΔE_Q = electric quadrupole splitting, Γ = experimental line width.

Sample	δ (mm•s^{-1})	ΔE_Q (mm•s^{-1})	Γ (mm•s^{-1})
LaMgSn	1.98(2)	0.93(1)	1.18(2)
LaMgSnH	1.99(1)	0.82(1)	1.09(2)

Table 4
^{119}Sn isomer shifts for various pairs of equiatomic stannides and their corresponding hydrides.

Stannide	Type	*T* (K)	δ (mm/s)	Hydride	δ (mm/s)	References
LaMgSn	TiNiSi	78	1.98(2)	LaMgSnH	1.99(1)	This work
ScNiSn	TiNiSi	78	1.773(1)	$ScNiSnH_{0.5}$	1.732(3)	[11]
LaNiSn	TiNiSi	293	1.888(7)	$LaNiSnH_2$	1.999(4)	[38]
CeNiSn	TiNiSi	293	1.900(7)	CeNiSnH	1.917(6)	[38]
CeRhSn	ZrNiAl	78	1.84(7)	$CeRhSnH_{0.8}$	1.87(2)	[39]
CePdSn	TiNiSi	293	1.89(1)	CePdSnH	1.94(1)	[40]
CeIrSn	ZrNiAl	78	1.76(3)	$CeIrSnH_{0.7}$	1.85(1)	[39]

hydrogen content make a precise correlation difficult. In any case, the ^{119}Sn isomer shifts precisely reflect the changing electronic situation at the tin nuclei.

Additionally, we need to consider the differences induced by the nature of the elements. La^{3+} and Mg^{2+} are closed-shell cations and we get the electron-precise description. The *d* elements and cerium are prone to different *f*-*d* hybridization and induce small changes in the electron density at the tin nuclei. This behaviour is also comparable to the pair CeRhSb and $CeRhSbH_{0.2}$ [41] studied by ^{121}Sb Mössbauer spectroscopy, where the Kondo semiconductor CeRhSb upon hydrogenation transforms to the $T_N = 3.6(2)$ K antiferromagnet $CeRhSbH_{0.2}$ paralleled by a decrease of the ^{121}Sb shift from –7.38(1) to –7.47(1) mm/s.

Studies on the corresponding cerium-based pair CeMgSn/CeMgSnH are under way in our group aimed at comparing these stannides with the corresponding lanthanum phases.

4. Concluding remarks

This work was aimed at studies of the effect of magnesium as a part of the chemical composition of the equiatomic intermetallic alloy LaMgSn with orthorhombic TiNiSi type of structure and the size of the interstitial sites occupied by hydrogen atoms on the hydrogenation behaviours and the properties of the hydrides formed. We have used LaNiSn intermetallic alloy forming a dihydride $LaNiSnH_2$ as a reference point.

Replacing Ni with Mg in the intermetallic compound LaNiSn causes a 23% volume expansion when forming LaMgSn, induced by the much larger size of the Mg atoms as compared to the Ni atoms. However, the crystal structure type - orthorhombic TiNiSi - remains unaltered. Tin creates strong bonds with the surrounding La atoms forming trigonal prisms [Sn@La_6]. Because of this, when the compound interacts with hydrogen at 200 °C under a pressure of 20 bar H_2 it forms an insertion mono-hydride, rather than disproportionating to the binary hydrides MgH_2 and $LaH_{2–3}$. However, LaMgSn shows a lower hydrogen storage capacity (1 at.H/f.u.) than the dihydride $LaNiSnH_2$ [3]. A computational study of the LaMgSn-H_2 system shows that the formation of the mono-hydride LaMgSnH is much more thermodynamically favourable compared to that of the dihydride $LaMgSnH_2$. However, formation of $LaMgSnH_2$ from LaMgSn remains possible as a thermodynamic driving force for the transformation LaMgSn → $LaMgSnH_2$ does exist, and might be activated at higher hydrogenation pressures.

Hydrogen is more strongly bound in LaMgSnH as compared to $LaNiSnH_2$ [3], as the peak of hydrogen vacuum desorption for the Mg-containing hydride is observed at 355 °C, while for $LaNiSnH_2$

hydrogen desorption starts at 130 °C and reaches its maximum at 325 °C. This is not surprising, as magnesium is an active hydride-forming metal while nickel is a transition metal which forms its binary monohydride when applying a kbar level of hydrogen pressures only.

Metal-H distances in LaMgSnH show shorter La−H bonds (2.38 and 2.50 Å) compared to $LaNiSnH_2$, 2.61 Å. This is because the Ni−H distances in the La_3Ni tetrahedra occupied by H in $LaNiSnH_2$, 1.619 Å, are much shorter than the Mg−D distances in the filled by D atoms La_3Mg tetrahedra of LaMgSnD, 2.026 Å.

The size of the La_3Mg interstices occupied by hydrogen (r = 0.54 Å) is smaller than the empty Mg_3La tetrahedral sites (r = 0.72 Å). This means that the sites occupied by H atoms should have an optimal size to become favourable for the accommodation of hydrogen atoms, and too large interstitials as Mg_3La tetrahedra are not favoured for the accommodation of H atoms. Earlier a preferable occupancy by H atoms of the interstices having a similar range of radii $0.48 \leq r \leq 0.53$ Å as for the La_3Mg sites has been observed for the saturated hydrides $Zr_3FeD_{6.7}$ [42,43] and $Zr_2FeD_{5.0}$ [43,44]. Thus, the structural chemistry of LaMgSnH/D resembles the typical for the intermetallic hydride dependencies.

We believe that the variation in the electronic density is the factor controlling occupancy by H atoms of the particular sites, further to the size factor. A higher local electronic density in the La_3Mg sites assists the creation of the bonds with H atoms and favours H insertion into the La-rich La_3Mg tetrahedra while preventing H insertion into the Mg-rich Mg_3La sites which are deficient in electronic density.

This paper is a part of a Virtual Special Issue of Journal of Alloys and Compounds dedicated to the memory of a late Prof. Vitalij K. Pecharsky who left us too early. Vitalij will be remembered for his contribution to the materials science, including his works on the metal hydrides as the materials for the reversible hydrogen storage. Among others, these works covered his studies of the hydrides containing light elements, aluminium, boron and nitrogen - alane and alanates [45–47], borohydrides [48] and amides [49]. He was one of the fond and successful users of the mechanochemical methods of synthesis and modification of the properties of the metal hydrides.

We will remember Vitalij as a warm and sincere colleague and friend who was leading the Journal of Alloys and Compounds as the Editor-in-Chief in the dissemination of the research outcome dedicated to hydrogen and energy storage. We will miss Vitalij and will keep him in our grateful memories.

Author statement

The manuscript STRUCTURE AND BONDING IN TiNiSi TYPE LaMgSnH INTERMETALLIC HYDRIDE has been jointly prepared by all co-authors, Volodymyr A. Yartys, Roman V. Denys, Lev G. Akselrud, Ponniah Vajeeston, Robert Dankelman, Jeroen Plomp, Theresa Block, Rainer Pöttgen, David Wragg, Bruno Guilherme Fischer Eggert, Vasyl Berezovets, who reviewed and approved its content.

CRediT authorship contribution statement

Block Theresa: Data curation, Investigation, Visualization, Writing – original draft, Writing – review & editing. **Plomp Jeroen:** Data curation, Writing – original draft. **Wragg David:** Data curation, Writing – original draft. **Pöttgen Rainer:** Investigation, Methodology, Supervision, Writing – original draft, Writing – review & editing. **Berezovets Vasyl:** Formal analysis, Visualization, Writing – review & editing. **Fischer Eggert Bruno Guilherme:** Data curation, Writing – original draft. **Denys Roman V.:** Data curation, Formal analysis, Visualization, Writing – original draft. **Yartys Volodymyr A.:** Project administration, Supervision, Writing – original draft, Writing – review & editing. **Vajeeston Ponniah:** Formal analysis, Investigation, Visualization, Writing – original draft, Writing – review & editing. **Akselrud Lev G.:** Formal analysis, Software, Visualization, Writing – original draft. **Dankelman Robert:** Data curation, Writing – original draft.

Declaration of Competing Interest

The authors declare no known competing financial interests or personal relationships that could have appeared to influence the work reported in this paper.

Data availability

Data will be made available on request.

Acknowledgements

This work has received a support from EU Horizon 2020 programme in the frame of the H2020-MSCA RISE-2017 action, HYDRIDE4MOBILITY project, with Grant Agreement 778307 (VAY and RVD). VAY acknowledges a support from the Institute for Energy Technology.

The authors appreciate the possibility to collect the SR XRD diffraction data at BM01, SNBL, ESRF, Grenoble, France and NPD data at Delft Reactor Institute, TU Delft, the Netherlands.

Appendix A. Supporting information

Supplementary data associated with this article can be found in the online version at doi:10.1016/j.jallcom.2023.173198.

References

[1] R.-D. Hoffmann, R. Pöttgen, 2001. AlB2 Related Intermetallic Compounds – A Comprehensive View Based on Group-Subgroup Relations, Z. Kristallogr. 216. 127–145.
[2] R. Pöttgen, Coloring, distortions and puckering in selected intermetallic structures from the perspective of group-subgroup relations, Z. Anorg. Allg. Chem. 640 (2014) 869–891, https://doi.org/10.1002/zaac.201400023.
[3] Sachin Gupta, Chapter 1 - Magnetic phenomena in equiatomic ternary rare earth compounds. Handbook of Magnetic Materials 32, 2023, pp. 1–103, https://doi.org/10.1016/bs.hmm.2023.09.001.
[4] Sachin Gupta, K.G. Suresh, Review on magnetic and related properties of RTX compounds, J. Alloy. Compd. 618 (2015) 562–606, https://doi.org/10.1016/j.jallcom.2014.08.079.
[5] Oliver Janka, Oliver Niehaus, Rainer Pöttgen, Bernard Chevalier, Cerium intermetallics with TiNiSi-type structure, Z. Nat. 71B (7) (2016) 737–764, https://doi.org/10.1515/znb-2016-0101.
[6] V.A. Yartys, T. Olavesen, B.C. Hauback, H. Fjellvåg, H.W. Brinks, Hexagonal $LaNiSnD_2$ with filled ZrBeSi-type structure, J. Alloy. Compd. 330–332 (2002) 141, https://doi.org/10.1016/S0925-8388(01)01523-7.
[7] H.W. Brinks, V.A. Yartys, B.C. Hauback, The crystal structure of $TbNiSiD_{1.78}$, J. Alloy. Compd. 322 (1-2) (2001) 160–165, https://doi.org/10.1016/S0925-8388(01)01013-1.
[8] V.A. Yartys, B. Ouladdiaf, O. Isnard, O.Yu Khyzhun, K.H.J. Buschow, Hydrogen induced antiferromagnetism in the Kondo semimetal CeNiSn, J. Alloy. Compd. 359 (1-2) (2003) 62–65, https://doi.org/10.1016/S0925-8388(03)00207-X.
[9] V.A. Yartys, T. Olavesen, B.C. Hauback, H. Fjellvåg, Orthorhombic NdNiSnD with filled TiNiSi-type structure, J. Alloy. Compd. 336 (1-2) (2002) 181–186, https://doi.org/10.1016/S0925-8388(01)01877-1.
[10] V.A. Yartys, R.V. Denys, O. Isnard, R.G. Delaplane, R. Svedlindh, K.H.J. Buschow, Crystal and magnetic structure of TbNiSnD studied by neutron powder diffraction, J. Magn. Magn. Mater. 311 (2007) 639–643, https://doi.org/10.1016/j.jmmm.2006.08.043.
[11] V.A. Yartys, V. Berezovets, L.G. Akselrud, V. Antonov, V. Fedotov, S. Klenner, R. Pöttgen, P. Vajeeston, D. Chernyshov, M. Heere, R.V. Denys, L. Havela, Hydrogen induced structural phase transformation in ScNiSn-based intermetallic hydride characterized by experimental studies and by a theoretical modelling, Acta Mater. 244 (2023), 118549, https://doi.org/10.1016/j.actamat.2022.118549.
[12] B. Chevalier, M. Pasturel, J.-L. Bobet, F. Weill, R. Decourt, J. Etourneau, The new hydrides $CeNiGeH_{1.6}$ and $CeCuGeH_{1.0}$ crystallizing in the derivative hexagonal ZrBeSi-type structure, J. Solid State Chem. 177 (2004) 752–759, https://doi:10.1016/j.jssc.2003.09.003.
[13] B. Chevalier, M. Pasturel, J.-L. Bobet, J. Etourneau, O. Isnard, J. Sanchez Marcos, J. Rodriguez Fernandez, Magnetic ordering induced by the hydrogenation of the ternary stannide CeNiSn, J. Magn. Magn. Mater. 272–276 (2004) 576–578, https://doi.org/10.1016/j.jmmm.2003.11.222.
[14] F. Weill, M. Pasturel, J.-L. Bobet, B. Chevalier, Ordering phenomena in intermetallic CeMX (M=Ni, Cu and X=Si, Ge, Sn) upon hydrogenation, J. Phys. Chem. Sol. 67 (2006) 1111–1116, https://doi.org/10.1016/j.jpcs.2006.01.032.

[15] A.M. Adamska, L. Havela, Y. Skourski, A.V. Andreev, Variations of structure and magnetic properties in UTGe hydrides (T = late transition metal), J. Alloy. Compd. 515 (2012) 171–179, https://doi.org/10.1016/j.jallcom.2011.11.131.

[16] Anna Adamska, Ladislav Havela, Karl Eichinger, Ji.ř.í Pospíšil, Khrystyna Miliyanchuk, Magnetic properties of the hydrogenated unconventional superconductor UCoGe–H (formerly Z. Metallkd.), Int. J. Mat. Res. 100 (9) (2009) 1230–1233, https://doi.org/10.3139/146.110177.

[17] P. Raj, K. Shashikala, A. Sathyamoorthy, Hydride phases, structure, and magnetic properties of the $UNiAlH_y$ system, Phys. Rev. B 63 (2001), 094414, https://doi.org/10.1103/PhysRevB.63.094414.

[18] P. Manfrinetti, A. Provino, K.A. Gschneidner Jr, On the RMgSn rare earth compounds, J. Alloy. Compd. 482 (2009) 81–85, https://doi.org/10.1016/j.jallcom.2009.03.178.

[19] S. Suwarno, M.V. Lototskyy, V.A. Yartys, Thermal desorption spectroscopy studies of hydrogen desorption from rare earth metal trihydrides REH_3 (RE = Dy, Ho, Er), J. Alloy. Compd. 842 (2020), 155530, https://doi.org/10.1016/j.jallcom.2020.155530.

[20] V. Dyadkin, P. Pattison, V. Dmitriev, D. Chernyshov, A new multipurpose diffractometer PILATUS@SNBL, J. Synchr. Rad. 23 (3) (2016) 825–829, https://doi.org/10.1107/S1600577516002411.

[21] L. van Eijck, L.D. Cussen, G.J. Sykora, E.M. Schooneveld, N.J. Rhodes, A.A. van Well, C. Pappas, Design and performance of a novel neutron powder diffractometer: PEARL at TU Delft, J. Appl. Crystallogr. 49 (5) (2016) 1398–1401, https://doi.org/10.1107/S160057671601089X.

[22] L. Akselrud, Yu Grin, WinCSD: software package for crystallographic calculations (Version 4), J. Appl. Crystallogr. 47 (2014) 803–805, https://doi.org/10.1107/S1600576714001058.

[23] R.A. Brand, WinNormos for Igor6 (version for Igor 6.2 or above: 22/02/2017), Universität Duisburg, Duisburg (Germany), 2017.

[24] CorelDRAW Graphics Suite 2017 (version 19.0.0.328), Corel Corporation: Ottawa, Ontario (Canada), 2017.

[25] G. Kresse, M. Marsman, J. Furthmüller. Vienna Ab-Initio Package Vienna Simulation: VASP the GUIDE; VASP Man, 2014; p 237. https://www.yumpu.com/user/cms.mpi.univie.ac.at.

[26] G. Sun, J. Kürti, P. Rajczy, M. Kertesz, J. Hafner, G. Kresse, Performance of the Vienna ab initio simulation package (VASP) in chemical applications, J. Mol. Struct. 624 (2003) 37–45, https://doi.org/10.1016/s0166-1280(02)00733-9.

[27] P. Hohenberg, W. Kohn, Inhomogeneous electron gas, Phys. Rev. 136 (1964) B864, https://doi.org/10.1103/physrev.136.b864.

[28] W. Kohn, L.J. Sham, Self-consistent equations including exchange and correlation effects, Phys. Rev. 140 (1965) A1133, https://doi.org/10.1103/physrev.140.a1133.

[29] J.P. Perdew, K. Burke, M. Ernzerhof, Generalized gradient approximation made simple, Phys. Rev. Lett. 77 (1996) 3865, https://doi.org/10.1103/physrevlett.77.3865.

[30] G. Kresse, D. Joubert, From ultrasoft pseudopotentials to the projector augmented-wave method, Phys. Rev. B 59 (1999) 1758, https://doi.org/10.1103/physrevb.59.1758.

[31] P.E. Blöchl, Projector augmented-wave method, Phys. Rev. B 50 (1994) 17953–17979, https://doi.org/10.1103/physrevb.50.17953.

[32] P. Vajeeston, P. Ravindran, C. Ravi, R. Asokamani, 2001. Phys. Rev. B 63 045115. https://doi.org/10.1103/PhysRevB.63.045115.

[33] V.A. Yartys, R.V. Denys, J.P. Maehlen, C.J. Webb, E.MacA.. Gray, T. Blach, A.A. Poletaev, J.K. Solberg, O. Isnard. Nanostructured Metal Hydrides for Hydrogen Storage Studied by In Situ Synchrotron and Neutron Diffraction, in In-Situ and Operando Probing of Energy Materials at Multiscale Down to Single Atomic Column—The Power of X-Rays, Neutrons and Electron Microscopy, edited by C.M. Wang, N. de Jonge, R.E. Dunin-Borkowski, A. Braun, J-H. Guo, H. Schober, R.E. Winans (Mater. Res. Soc. Symp. Proc. Volume 1262, Warrendale, PA, 2010), Paper #: 1262-W04–01. https://doi.org/10.1557/PROC-1262-W04–01. ISBN: 978–1-60511–239-8.

[34] R.V. Denys, A.B. Riabov, J.P. Maehlen, M.V. Lototsky, J.K. Solberg, V.A. Yartys, In situ synchrotron X-ray diffraction studies of hydrogen desorption and absorption properties of Mg and Mg-Mm-Ni after reactive ball milling in hydrogen, Acta Mater. 57 (13) (2009) 3989–4000, https://doi.org/10.1016/j.actamat.2009.05.004.

[35] T. Del Rose, R. Choudhary, Ya Mudryk, D. Haskel, A.K. Pathak, G. Bhaskar, J. V. Zaikina, D.D. Johnson, V.K. Pecharsky, Interplay between Kondo and magnetic interactions in $Pr_{0.75}Gd_{0.25}ScGeH$, J. Alloy. Compd. 966 (2023), 171351, https://doi.org/10.1016/j.jallcom.2023.171351.

[36] R. Pöttgen, Stannides and intermetallic tin compounds – fundamentals and applications, Z. Nat. 61b (2006) 677–698, https://doi.org/10.1515/znb-2006-0607.

[37] R.-D. Hoffmann, D. Kußmann, U.Ch Rodewald, R. Pöttgen, C. Rosenhahn, B. D. Mosel, New Stannides $CaTSn_2$ (T = Rh, Pd, Ir) and $Ca_2Pt_3Sn_5$ – synthesis, structure, and chemical bonding, Z. Nat. 54b (1999) 709–717, https://doi.org/10.1515/znb-1999-0602.

[38] B. Chevalier, A. Wattiaux, L. Fournès, M. Pasturel, ^{119}Sn Mössbauer spectroscopy studies of hydrides deriving from the stannide CeNiSn, Solid State Sci. 6 (2004) 573–577, https://doi.org/10.1016/j.solidstatesciences.2004.03.008.

[39] B. Chevalier, C.P. Sebastian, R. Pöttgen, Hydrogenation of the intermediate valence ternary stannides CeRhSn and CeIrSn, Solid State Sci. 8 (2006) 1000–1008, https://doi.org/10.1016/j.solidstatesciences.2006.02.047.

[40] B. Chevalier, A. Wattiaux, J.-L. Bobet, The Doniach diagram and hydrogenation of the ternary compounds CePdIn and CePdSn, J. Phys.: Condens. Matter 18 (2006) 1743–1755, https://doi.org/10.1088/0953-8984/18/5/026.

[41] B. Chevalier, R. Decourt, B. Heying, F.M. Schappacher, U.Ch. Rodewald, R. D. Hoffmann, R. Pöttgen, R. Eger, A. Simon, Inducing magnetism in the Kondo semiconductor CeRhSb through hydrogenation – antiferromagnetic behaviour of the new hydride CeRhSbH0.2. Chem. Mater. 19 (2007) 28–35. https://doi.org/10.1021/cm062168a.

[42] V.A. Yartys, H. Fjellvåg, B.C. Hauback, A.B. Riabov, Neutron diffraction studies of Zr-containing intermetallic hydrides with ordered hydrogen sublattice I. Crystal structure of Zr2FeD5, J. Alloy. Compds 274 (1998) 217–221.

[43] V.A. Yartys, H. Fjellvåg, I.R. Harris, B.C. Hauback, A.B. Riabov, M.H. Sørby, I. Yu Zavaliy, Hydrogen ordering and H-induced phase transformations in Zr-based intermetallic hydrides, J. Alloy. Compd. 293–295 (1999) 74–87, https://doi.org/10.1016/S0925-8388(99)00304-7.

[44] V.A. Yartys, H. Fjellvåg, B.C. Hauback, A.B. Riabov, M.H. Sørby, Neutron diffraction studies of Zr-containing intermetallic hydrides with ordered hydrogen sublattice. II. Orthorhombic $Zr_3FeD_{6.7}$ with filled Re_3B-type structure, J. Alloy. Compd. 278 (1–2) (1998) 252–259.

[45] Viktor P. Balema, Kevin W. Dennis, Vitalij K. Pecharsky, Rapid solid-state transformation of tetrahedral $[AlH_4]^-$ into octahedral $[AlH_6]^{3-}$ in lithium aluminohydride, Chem. Commun. (17) (2000) 1665–1666, https://doi.org/10.1039/B004144K.

[46] V.P. Balema, V.K. Pecharsky, K.W. Dennis, Solid state phase transformations in LiAlH4 during high-energy ball-milling, J. Alloy. Compd. 313 (1–2) (2000) 69–74, https://doi.org/10.1016/S0925-8388(00)01201-9.

[47] Ihor Z. Hlova, Shalabh Gupta, Jennifer F. Goldston, Takeshi Kobayashi, Marek Pruski, Vitalij K. Pecharsky, Dry mechanochemical synthesis of alane from LiH and $AlCl_3$, Faraday Discuss. 170 (2014) 137–153, https://doi.org/10.1039/C3FD00161J.

[48] Oleksandr Dolotko, Shalabh Gupta, Takeshi Kobayashi, Eric McDonald, Ihor Hlova, Eric Majzoub, Viktor P. Balema, Marek Pruski, Vitalij K. Pecharsky, Mechanochemical reactions and hydrogen storage capacities in MBH_4–SiS_2 systems (M= Li or Na), Int. J. Hydr. Energy 44 (14) (2019) 7381–7391, https://doi.org/10.1016/j.ijhydene.2019.01.211.

[49] Oleksandr Dolotko, Neil Paulson, Vitalij K. Pecharsky, Thermochemical transformations in $2MNH_2$–$3MgH_2$ systems (M= Li or Na), Int. J. Hydr. Energy 35 (10) (2010) 4562–4568, https://doi.org/10.1016/j.ijhydene.2010.02.104.